Automatica 54 (2015) 146–157

Contents lists available at ScienceDirect

Automatica

journal homepage: www.elsevier.com/locate/automatica

Output feedback stabilization of inverted pendulum on a cart in the presence of uncertainties☆

Joonho Lee [a], Ranjan Mukherjee [a], Hassan K. Khalil [b]

[a] Department of Mechanical Engineering, Michigan State University East Lansing, MI 48823, USA
[b] Department of Electrical and Computer Engineering, Michigan State University East Lansing, MI 48823, USA

ARTICLE INFO

Article history:
Received 19 March 2014
Received in revised form
15 September 2014
Accepted 21 December 2014
Available online 20 February 2015

Keywords:
Extended High-Gain Observers
Dynamic inversion
Underactuated mechanical systems

ABSTRACT

An output feedback controller is proposed for stabilization of the inverted pendulum on a cart in the presence of uncertainties. The output feedback controller has a multi-time-scale structure in which Extended High-Gain Observers are used to estimate system states and uncertainties in the first and fastest time scale; dynamic inversion is used to deal with uncertain input coefficients in the second time scale; the pendulum converges to a reference trajectory in the third time scale; and finally, the reference trajectory is designed such that both the pendulum and the cart converge to the desired equilibrium in the fourth and slowest time scale. The multi-time-scale structure allows independent analysis of the dynamics in each time scale and singular perturbation methods are effectively utilized to establish exponential stability of the equilibrium. Simulation results indicate that the output feedback controller provides a large region of attraction and experimental results establish the feasibility of practical implementation.

1. Introduction

An inverted pendulum on a cart is a classical example of an underactuated mechanical system and its stabilization problem has been investigated by many researchers. Based on linearized system dynamics, controllers can be designed to stabilize the equilibrium but the size of the region of attraction is typically small. Furthermore, these controllers are not very effective in the presence of significant uncertainties in the system model. In this paper we present an output feedback control design that can stabilize the equilibrium in the presence of significant uncertainties and provide a large region of attraction.

One representative approach for stabilization of the inverted pendulum on a cart is based on the energy of the system. Spong and Praly (1996) used partial feedback linearization to linearize the cart dynamics followed by transfer of energy from the cart to the pendulum. A stabilizing controller is invoked when the configuration of the system reaches a neighborhood of the equilibrium. Astrom and Furuta (2000) used a Lyapunov function based on the potential energy of the pendulum, and Lozano, Fantoni, and Block (2000) stabilized the pendulum around its homoclinic orbit prior to stabilization. Fradkov (1996) developed a control method using an energy-based objective function and the speed-gradient, and Shiriaev, Egeland, Ludvigsen, and Fradkov (2001) proposed a modified controller using the idea of variable structure systems. Muralidharan, Ravichandran, and Mahindrakar (2009) designed a controller for the two-wheeled inverted pendulum using the interconnection and damping-passivity-based control (IDA-PBC) method proposed by Ortega, Spong, Gomez-Estern, and Blankenstein (2002) for underactuated systems. Sarras, Acosta, Ortega, and Mahindrakar (2013) combined the approach of the Immersion and Invariance proposed by Astolfi, Karagiannis, and Ortega (2007) with the Hamiltonian formulation to accommodate underactuation degree greater than one. Bloch, Chang, Leonard, and Marsden (2001); Bloch, Leonard, and Marsden (2000) used the controlled Lagrangian approach to derive a desired closed-loop system dynamics for stabilization. The controller is designed by matching the dynamic equations for the uncontrolled and controlled Lagrangians. In Bloch et al. (2000), only the kinetic energy was shaped to obtain the desired dynamics whereas both kinetic and potential energies were shaped in Bloch et al. (2001). Angeli (2001) developed a smooth feedback law for almost-global stabilization based on the energy-shaping control strategy in

☆ This work was supported in part by the National Science Foundation under grant numbers ECCS-1128467 and CMMI-0925055. The material in this paper was not presented at any conference. This paper was recommended for publication in revised form by Associate Editor Hiroshi Ito under the direction of Editor Andrew R. Teel.

E-mail addresses: leejoon8@msu.edu (J. Lee), mukherji@egr.msu.edu (R. Mukherjee), khalil@msu.edu (H.K. Khalil).

http://dx.doi.org/10.1016/j.automatica.2015.01.013
0005-1098/

Bloch et al. (2000). Auckly, Kapitanski, and White (2000) derived a stabilizing controller by solving a set of linear partial differential equations; these equations were obtained by matching the desired closed-loop system dynamics based on the potential energy with the original dynamics.

Among other approaches, Mazenc and Praly (1996) and Teel (1996) developed control methods based on the concept of interconnected systems. In Mazenc and Praly (1996), the stability analysis was carried out using a Lyapunov function whereas in Teel (1996) a nonlinear small gain theorem was used. Olfati-Saber (2002) proposed a transformation to convert the system into cascade normal form, for which existing control methods can be used for stabilization. A two-time-scale approach was proposed by Getz and Hedrick (1995) and Srinivasan, Huguenin, and Bonvin (2009). In Getz et al. (1995), the trajectories of the pendulum were rapidly converged to a reference trajectory and the reference trajectory was slowly varied to converge the cart to its desired position. In Srinivasan et al. (2009), low gains were used near the equilibrium for separation of time scales. All of the methods discussed above require exact knowledge of the system dynamics and are unlikely to guarantee stabilization in the presence of significant uncertainties.

To deal with uncertainties of the system model, Ravichandran and Mahindrakar (2011) used a two-time-scale approach together with Lyapunov redesign. However, the transient behavior of the fast system was not analyzed. Park and Chwa (2009) utilized two sliding surfaces for the pendulum and cart subsystems to stabilize the system in the presence of disturbances but uncertainties in system parameters were not considered. Adhikary and Mahanta (2013) used backstepping and sliding mode control to the normal form of the system. Both uncertainties and disturbances were considered but they were introduced after the system was converted into normal form. Xu, Guo, and Lee (2013) used integral sliding-mode control (Cao & Xu, 2004) to deal with uncertainties in the two-wheeled mobile inverted pendulum but the size of the region of attraction of the equilibrium is small since the controller is designed based on the linearized system dynamics.

In this paper we present an output feedback controller to stabilize the inverted pendulum on a cart in the presence of significant uncertainties. Extended High-Gain Observers and dynamic inversion are combined together with a multi-time-scale structure to deal with model uncertainties. The stability analysis for the multi-time-scale structure is carried out using singular perturbation methods; the advantage of this approach is that the behavior of the system can be analyzed independently for each time scale. The multi-time-scale structure of the controller effectively provides a large region of attraction and this is illustrated through simulations. Output feedback control of the inverted pendulum on a cart has not been proposed earlier and it is shown here that it can recover the performance of the system under state feedback.

The paper is organized as follows. In Section 2, a state feedback controller is designed using a two-time-scale structure; uncertainties are not considered. In Section 3, the output feedback controller is designed in the presence of uncertainties. Simulation and experimental results are presented in Section 4 and conclusions are provided in Section 5.

2. Stabilization in the absence of uncertainties

We present a control strategy to stabilize the desired equilibrium of the inverted pendulum on a cart system, in the absence of uncertainties. The controller is based on the designs proposed by Getz (1995) and Srinivasan et al. (2009); here we cast the closed-loop system dynamics in two-time scale format for the purpose of stability analysis. The stability analysis is done by transforming the system into a standard singularly perturbed one.

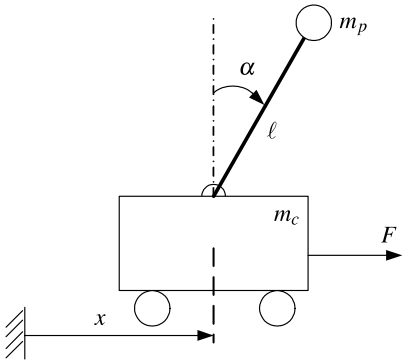

Fig. 1. Inverted pendulum on a cart.

Remark 1. As an intermediate step for the output feedback controller in Section 3, we design a controller in this section in the absence of uncertainties.

2.1. Dynamics of an inverted pendulum on a cart

The dynamics of an inverted pendulum on a cart are given by

$$\begin{bmatrix} m_p + m_c & \ell m_p \cos\alpha \\ \ell m_p \cos\alpha & \ell^2 m_p \end{bmatrix} \begin{bmatrix} \ddot{x} \\ \ddot{\alpha} \end{bmatrix} = \begin{bmatrix} \ell m_p \dot{\alpha}^2 \sin\alpha \\ g\ell m_p \sin\alpha \end{bmatrix} + \begin{bmatrix} F \\ 0 \end{bmatrix} \tag{1}$$

where m_p, m_c are masses of the pendulum and the cart, respectively; g is the acceleration due to gravity; and ℓ is the length of the pendulum—see Fig. 1. The variables x and α denote the position of the cart and the angular displacement of the pendulum, respectively; α is measured clockwise from the vertical following the notation in Getz (1995). The variable F denotes the force applied on the cart and is the control input. With the choice of state variables

$$x_1 = x, \qquad x_2 = \dot{x}, \qquad \alpha_1 = \alpha, \qquad \alpha_2 = \dot{\alpha}$$

the system equations of (1) take the form

$$\begin{aligned} &\dot{x}_1 = x_2, \qquad \dot{x}_2 = f_x(\alpha_1, \alpha_2, F), \qquad \dot{\alpha}_1 = \alpha_2, \\ &\dot{\alpha}_2 = f_\alpha(\alpha_1, \alpha_2, F) \end{aligned} \tag{2}$$

where

$$\begin{aligned} f_x &= \frac{1}{(m_p + m_c - m_p \cos^2\alpha_1)} F + G_x \\ f_\alpha &= \frac{-\cos\alpha_1}{\ell(m_p + m_c - m_p \cos^2\alpha_1)} F + G_\alpha \\ G_x &= \frac{(\ell m_p \alpha_2^2 \sin\alpha_1 - m_p g \cos\alpha_1 \sin\alpha_1)}{(m_p + m_c - m_p \cos^2\alpha_1)} \\ G_\alpha &= \left(\frac{g}{\ell}\right) \sin\alpha_1 - \frac{\cos\alpha_1}{\ell} G_x. \end{aligned} \tag{3}$$

We consider equations in (2) over the domain $x = [x_1, x_2]^T \in D_x$ and $\alpha = [\alpha_1, \alpha_2]^T \in D_\alpha$ where $D_x = \{-a_{x_1} < x_1 < a_{x_1}\} \times \{-a_{x_2} < x_2 < a_{x_2}\} \subset \mathbf{R}^2$ and $D_\alpha = \{-a_{\alpha_1} < \alpha_1 < a_{\alpha_1}\} \times \{-a_{\alpha_2} < \alpha_2 < a_{\alpha_2}\} \subset \mathbf{R}^2$ are bounded. The constants, a_{x_1}, a_{x_2}, a_{α_1}, and a_{α_2} are positive numbers and $a_{\alpha_1} < \pi/2$.

2.2. Control design

The choice of the control input

$$F = (m_c + m_p - m_p \cos^2\alpha_1)(u - G_x) \tag{4}$$

with

$$u = g \tan\alpha_1 - \left(\frac{\ell}{\cos\alpha_1}\right) \nu_d \tag{5}$$

results in

$$\dot{x}_1 = x_2$$
$$\dot{x}_2 = g\tan\alpha_1 - \left(\frac{\ell}{\cos\alpha_1}\right) v_d \tag{6}$$

$$\dot{\alpha}_1 = \alpha_2$$
$$\dot{\alpha}_2 = v_d. \tag{7}$$

We choose

$$v_d = -\beta_1(\alpha_1 - \alpha_r) - \beta_2\alpha_2 \tag{8}$$

where α_r is a reference trajectory for α_1, which will be chosen using the concept of equilibrium manifold (Getz, 1995).

The desired dynamics of the x-subsystem is

$$\dot{x}_1 = x_2$$
$$\dot{x}_2 = v_{ext} - \left(\frac{\ell}{\cos\alpha_1}\right) v_d \tag{9}$$

where v_{ext} is chosen as

$$v_{ext} = -\gamma_1 x_1 - \gamma_2 x_2 \tag{10}$$

and $(\ell/\cos\alpha_1)v_d$ is considered to be a vanishing perturbation. By comparing the actual x-subsystem in (6) with the desired x-subsystem in (9), the desired reference trajectory for α_r can be determined as follows:

$$g\tan\alpha_r = v_{ext} \Leftrightarrow \alpha_r = \tan^{-1}\left(\frac{v_{ext}}{g}\right). \tag{11}$$

The control input v_d in (8) can now be designed as follows:

$$v_d = -\beta_1\left[\alpha_1 - \tan^{-1}\left(\frac{v_{ext}}{g}\right)\right] - \beta_2\alpha_2. \tag{12}$$

2.3. Closed-loop system

Using (4), (5), and (8), the closed-loop system dynamics can be represented as

$$\dot{x}_1 = x_2$$
$$\dot{x}_2 = g\tan\alpha_1 + \left(\frac{\ell}{\cos\alpha_1}\right)[\beta_2\alpha_2 + \beta_1(\alpha_1 - \alpha_r)] \tag{13}$$
$$\dot{\alpha}_1 = \alpha_2$$
$$\dot{\alpha}_2 = -\beta_2\alpha_2 - \beta_1(\alpha_1 - \alpha_r).$$

The above system is comprised of two subsystems: the cart dynamics described by states x_1 and x_2, and the pendulum dynamics described by states α_1 and α_2. Through proper choice of β_1 and β_2, we can ensure that α_1 converges to α_r quickly and α_2 converges to 0. Then, the cart dynamics is described by

$$\dot{x}_1 = x_2$$
$$\dot{x}_2 = g\tan\alpha_r = v_{ext} = -\gamma_1 x_1 - \gamma_2 x_2 \tag{14}$$

which guarantees asymptotic stability of the origin $(x, \dot{x}) = (0, 0)$.

2.4. Analysis using singular perturbations

To make the cart dynamics slower than the pendulum dynamics, we choose low gains for the cart controller: $\gamma_1 = \varepsilon_1^2 k_1$ and $\gamma_2 = \varepsilon_1 k_2$, where ε_1 is a small positive parameter and positive constants k_1 and k_2 are independent of ε_1. We note that instead of using the low gains in the cart controller, high gains can be used in the pendulum controller. However, the use of high gains results in peaking in the slow dynamics. The change of variables

$$y = [y_1, y_2]^T, \qquad y_1 = \varepsilon_1^2 x_1, \qquad y_2 = \varepsilon_1 x_2 \tag{15}$$

$$\theta = [\theta_1, \theta_2]^T, \qquad \theta_1 = \alpha_1 - \alpha_r, \qquad \theta_2 = \alpha_2 \tag{16}$$

transforms the system (13) into the singularly perturbed form

$$\begin{aligned}
\dot{y}_1 &= \varepsilon_1 y_2 \\
\dot{y}_2 &= \varepsilon_1[-k_1 y_1 - k_2 y_2 + h_x(\theta, \alpha_r)] \\
\dot{\theta}_1 &= \theta_2 + \varepsilon_1 h_\alpha(y, \theta, \alpha_r, F) \\
\dot{\theta}_2 &= -\beta_1\theta_1 - \beta_2\theta_2
\end{aligned} \tag{17}$$

where h_x and h_α are given by the expressions

$$\begin{aligned}
h_x &= g\,[\tan(\theta_1 + \alpha_r) - \tan\alpha_r] \\
&\quad + \left[\frac{\ell}{\cos(\theta_1 + \alpha_r)}\right](\beta_1\theta_1 + \beta_2\theta_2)\,, \\
h_\alpha &= \left[\frac{g}{g^2 + (-k_1 y_1 - k_2 y_2)^2}\right](k_1 y_2 + k_2 f_x)
\end{aligned} \tag{18}$$

and f_x is defined in (3), except that α_1 should now be replaced by $(\theta_1 + \alpha_r)$ in accordance with (15). We note that h_x and h_α are bounded by constants independent of ε_1 for all $\varepsilon_1 \ll 1$ over the domains D_x and D_α. The boundary layer system is obtained by setting $\varepsilon_1 = 0$ in (17):

$$\dot{\theta} = A_\theta\theta, \quad A_\theta = \begin{bmatrix} 0 & 1 \\ -\beta_1 & -\beta_2 \end{bmatrix} \tag{19}$$

where β_1 and β_2 are chosen such that A_θ is Hurwitz. The reduced system is obtained by setting $\varepsilon_1 = 0$:

$$\dot{y} = \varepsilon_1 A_y y, \quad A_y = \begin{bmatrix} 0 & 1 \\ -k_1 & -k_2 \end{bmatrix} \tag{20}$$

where k_1 and k_2 are chosen such that A_y is Hurwitz. The two time-scale structure of the system is depicted in Fig. 2.

It follows from Theorem 11.4 of Khalil (2002) that there exists a positive constant ε_1^* such that for $\varepsilon_1 \in (0, \varepsilon_1^*)$ the origin of the closed-loop system (17) is exponentially stable.

The design of β_1 and β_2 should ensure that α_1 stays in the set $|\alpha_1| < a_{\alpha_1}$ where $a_{\alpha_1} < \pi/2$. Since $\theta_1 = \alpha_1 - \alpha_r = \alpha_1 - \tan^{-1}(v_{ext}/g)$, by choosing ε_1 small enough we can constrain θ_1 to the set $|\theta_1| \le b_{\theta_1}$ with $b_{\theta_1} < \pi/2$. The initial state $\theta(0)$ belongs to a compact set $\{|\theta_1| \le a_{\theta_1},\ \ |\theta_2| \le a_{\theta_2}\}$ where $a_{\theta_1} < \pi/2$ and a_{θ_2} is some positive constant. We are going to design β_1 and β_2 to obtain a Lyapunov function V_θ for the system:

$$\dot{\theta}_1 = \theta_2, \qquad \dot{\theta}_2 = -\beta_1\theta_1 - \beta_2\theta_2$$

such that the compact set $\{V_\theta \le c_\theta\}$ contains the set $\{|\theta_1| \le a_{\theta_1},\ \ |\theta_2| \le a_{\theta_2}\}$ and is contained in the strip $|\theta_1| \le b_{\theta_1}$ with $a_{\theta_1} < b_{\theta_1} < \pi/2$. By showing that $\dot{V}_\theta$ is negative definite we ensure that the set $\{V_\theta \le c_\theta\}$ is positively invariant and all trajectories starting in $\{|\theta_1| \le a_{\theta_1},\ \ |\theta_2| \le a_{\theta_2}\}$ stay in the strip $|\theta_1| \le b_{\theta_1}$ for all $t \ge 0$. The gains β_1 and β_2 are taken as $\beta_1 = (\beta_{c1}/\mu)$ and $\beta_2 = (\beta_{c2}/\mu)$ with positive constants β_{c1} and β_{c2}, and a small positive constant μ. The Lyapunov function is taken as

$$V_\theta = \tilde{\theta}^T P_\alpha \tilde{\theta}, \quad \tilde{\theta} = \begin{bmatrix} \theta_1 \\ \left(\frac{\beta_1}{\beta_2}\right)\theta_1 + \theta_2 \end{bmatrix}, \quad P_\alpha = \begin{bmatrix} \frac{1}{2} & 0 \\ 0 & \frac{d}{2} \end{bmatrix}. \tag{21}$$

By choosing $c_\theta < \frac{1}{2}b_{\theta_1}^2$ we have

$$V_\theta \le c_\theta \Rightarrow \frac{1}{2}\theta_1^2 \le c_\theta < \frac{1}{2}b_{\theta_1}^2 \Rightarrow |\theta_1| < b_{\theta_1}.$$

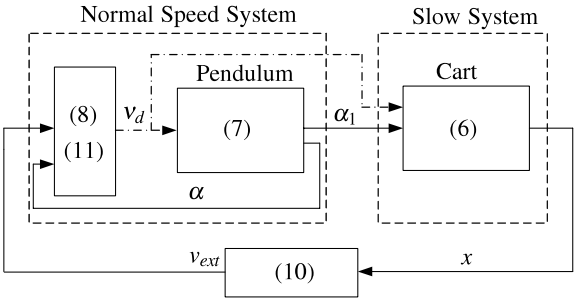

Fig. 2. The two-time-scale structure of the inverted pendulum on a cart system.

Over the set $\{|\theta_1| \le a_{\theta_1}, \quad |\theta_2| \le a_{\theta_2}\}$,

$$V_\theta \le \frac{1}{2}a_{\theta_1}^2 + \frac{d}{2}\left[\left(\frac{\beta_1}{\beta_2}\right)a_{\theta_1} + a_{\theta_2}\right]^2.$$

Therefore by choosing

$$d < \frac{(2c_\theta - a_{\theta_1}^2)}{\left[(\beta_1/\beta_2)a_{\theta_1} + a_{\theta_2}\right]^2}$$

we ensure that $\{|\theta_1| \le a_{\theta_1}, \quad |\theta_2| \le a_{\theta_2}\} \subset \{V_\theta \le c_\theta\}$. As in standard analysis of singularly perturbed systems (Theorem 2.1 of Chapter 7.2 of Kokotovic, Khalil, & O'Reilly, 1986), the derivative $\dot{V}_\theta$ will be negative definite by choosing μ sufficiently small.

3. Stabilization in the presence of uncertainties

In the presence of parameter uncertainties, f_x and f_α of (2) are unknown. We however note that the following conditions (the sign of the input coefficients in (3)) hold in D_x and D_α:

$$\begin{aligned} &\text{sign}(c_x) > 0, \quad c_x = \frac{1}{m_p + m_c - m_p\cos^2\alpha_1} \\ &\text{sign}(c_\alpha) > 0, \quad c_\alpha = \frac{c_x\cos\alpha_1}{\ell}. \end{aligned} \tag{22}$$

Extended High-Gain Observers will be used to estimate the uncertain terms in f_x and f_α in addition to the states; and dynamic inversion will be used to compute the inputs F and u, described by (4) and (5), using the estimates of f_x and f_α.

3.1. Dynamic inversion

With the knowledge of the sign of the input coefficients, as shown in (22), we use a dynamic inversion scheme which is different from ones in Getz (1995) and Hovakimyan, Lavretsky, and Cao (2008); Hovakimyan, Lavretsky, and Sasane (2005), in order to compute the control inputs F and u. The proposed dynamic inversion scheme in the paper is an extension in our earlier work (Lee, Mukherjee, & Khalil, 2012) since our earlier work dealt with SISO systems. In particular, had f_x and f_α been known, we could have used

$$\varepsilon_2\begin{bmatrix}\dot{F}\\ \dot{u}\end{bmatrix} = \begin{bmatrix}-f_x + u\\ f_\alpha - \nu_d\end{bmatrix} \tag{23}$$

to solve for F and u, starting from arbitrary initial conditions. In the above equation, ε_2 is a small positive number; its relationship with ε_1 will be discussed later. As $\varepsilon_2 \to 0$ and the stability of (23) is guaranteed, $f_x \approx u$ and $f_\alpha \approx \nu_d$. Eq. (23) is a singularly perturbed system of the form

$$\varepsilon_2\begin{bmatrix}\dot{F}\\ \dot{u}\end{bmatrix} = A_z\begin{bmatrix}F\\ u\end{bmatrix} + \begin{bmatrix}G_x\\ G_\alpha - \nu_d\end{bmatrix}, \qquad A_z = \begin{bmatrix}-c_x & 1\\ -c_\alpha & 0\end{bmatrix} \tag{24}$$

whose quasi-steady-state solution is given by (4) and (5). Since the foregoing equation is linear in F and u and the matrix A_z with frozen x and α is Hurwitz, it can be seen that for sufficiently small ε_2, F and u converge fast to their values that satisfy (4) and (5). The stability analysis for the system in (24) will be discussed in Section 3.

Remark 2. The dynamic inversion scheme used in this section is different from ones in Getz (1995) and Hovakimyan et al. (2008, 2005).

- In Getz (1995) and Hovakimyan et al. (2008), the dynamic inversion schemes were developed by the Jacobian with respect to inputs whereas the proposed one in the paper is based on the stability of the fast dynamics in (24), which only requires the knowledge on the signs of inputs.
- In Getz (1995), the stability analysis for the dynamic inversion is limited to a local neighborhood of the equilibrium, whereas our stability analysis is based on Lyapunov functions, which covers a larger domain than one in Getz (1995).
- In Hovakimyan et al. (2005), the dynamic inversion is only for SISO systems whereas our dynamic inversion scheme is able to deal with MIMO systems since the dynamic inversion has the inputs F and u in (24).

3.2. Extended High-Gain Observers (EHGOs)

Now, we assume that velocity and acceleration terms, x_2, α_2, $\sigma_x(x, \alpha, u)$, and $\sigma_\alpha(x, \alpha, u)$, which are used in the dynamic inversion, are unknown. EHGOs are designed to estimate the acceleration and velocity terms. The EHGOs for the cart and pendulum systems are designed as

$$\begin{aligned}
\dot{\hat{x}}_1 &= \hat{x}_2 + \left(\frac{h_{11}}{\varepsilon_3}\right)(x_1 - \hat{x}_1)\\
\dot{\hat{x}}_2 &= \bar{f}_x(\hat{\alpha}_1, \hat{\alpha}_2, F) + \hat{\sigma}_x + \left(\frac{h_{12}}{\varepsilon_3^2}\right)(x_1 - \hat{x}_1)\\
\dot{\hat{\sigma}}_x &= \left(\frac{h_{13}}{\varepsilon_3^3}\right)(x_1 - \hat{x}_1)\\
\dot{\hat{\alpha}}_1 &= \hat{\alpha}_2 + \left(\frac{h_{21}}{\varepsilon_3}\right)(\alpha_1 - \hat{\alpha}_1)\\
\dot{\hat{\alpha}}_2 &= \bar{f}_\alpha(\hat{\alpha}_1, \hat{\alpha}_2, F) + \hat{\sigma}_\alpha + \left(\frac{h_{22}}{\varepsilon_3^2}\right)(\alpha_1 - \hat{\alpha}_1)\\
\dot{\hat{\sigma}}_\alpha &= \left(\frac{h_{23}}{\varepsilon_3^3}\right)(\alpha_1 - \hat{\alpha}_1)
\end{aligned} \tag{25}$$

where $\bar{f}_x$ and $\bar{f}_\alpha$ are the nominal values of f_x and f_α in (3); $\hat{\sigma}_x$ and $\hat{\sigma}_\alpha$ denote the estimates of σ_x and σ_α, which are the uncertainties in the values of f_x and f_α, respectively, i.e. $f_x = \bar{f}_x + \sigma_x$ and $f_\alpha = \bar{f}_\alpha + \sigma_\alpha$. The constants h_{ij} for $i = 1, 2$ and $j = 1, 2, 3$ are chosen such that the following polynomials

$$s^3 + h_{i1}s^2 + h_{i2}s + h_{i3}, \quad \text{for } i = 1, 2$$

are Hurwitz and ε_3 is a small positive number.

Remark 3. The parameters ε_1, ε_2 and ε_3 should satisfy $\varepsilon_1 \ll 1$, $\varepsilon_2 \ll 1$, and $(\varepsilon_3/\varepsilon_2) \ll 1$. This requirement can be intuitively explained as follows. Since the EHGOs' estimates $\hat{\sigma}_x$ and $\hat{\sigma}_\alpha$ are used in dynamic inversion, the observer dynamics should be faster than the dynamic inversion algorithm; hence, $(\varepsilon_3/\varepsilon_2) \ll 1$. Since the dynamic inversion computes u and F, which are used to implement the controller, its dynamics should be faster than the dynamics of the closed-loop system with no uncertainty (13); hence $\varepsilon_2 \ll 1$. Since the x-dynamics is much slower than the α-dynamics, $\varepsilon_1 \ll 1$.

3.3. Output feedback control

Using the dynamic inversions together with the EHGOs, the output feedback control is

$$\varepsilon_2 \begin{bmatrix} \dot{F} \\ \dot{u} \end{bmatrix} = \begin{bmatrix} -\bar{f}_x\left(\alpha_1, M_\theta \text{sat}\left(\frac{\hat{\alpha}_2}{M_\theta}\right), F\right) - M_x \text{sat}\left(\frac{\hat{\sigma}_x}{M_x}\right) + u \\ \bar{f}_\alpha\left(\alpha_1, M_\theta \text{sat}\left(\frac{\hat{\alpha}_2}{M_\theta}\right), F\right) + M_\alpha \text{sat}\left(\frac{\hat{\sigma}_\alpha}{M_\alpha}\right) - \hat{v}_d \end{bmatrix} \tag{26}$$

where

$$\begin{aligned} \hat{v}_d &= -\beta_1(\alpha_1 - \hat{\alpha}_r) - \beta_2 M_\theta \text{sat}\left(\frac{\hat{\alpha}_2}{M_\theta}\right), \\ \hat{\alpha}_r &= \tan^{-1}\left(\frac{\hat{v}_{ext}}{g}\right), \\ \hat{v}_{ext} &= -\gamma_1 x_1 - \gamma_2 \hat{x}_2. \end{aligned} \tag{27}$$

To protect the system from peaking, the saturation function $\text{sat}(\cdot)$

$$\text{sat}(e) = \begin{cases} e, & \text{if } |e| \le 1 \\ \text{sign}(e), & \text{if } |e| > 1 \end{cases}$$

is used. The saturation limits M_x, M_α, and M_θ are determined such that the saturation functions will not be invoked under state feedback.

3.4. Stability analysis in the presence of uncertainties

The closed-loop system is represented in the singularly perturbed form

$$\begin{aligned} \dot{y}_1 &= \varepsilon_1 y_2 \\ \dot{y}_2 &= \varepsilon_1 f_x\left(\theta_1 + \alpha_r, \theta_2, F\right) \end{aligned} \tag{28}$$

$$\begin{aligned} \dot{\theta}_1 &= \theta_2 + \varepsilon_1 h_\alpha(y, \theta, \alpha_r, F) \\ \dot{\theta}_2 &= f_\alpha\left(\theta_1 + \alpha_r, \theta_2, F\right) \end{aligned} \tag{29}$$

$$\varepsilon_2 \dot{z} = A_z z + \psi(\cdot) - \varepsilon_2 \phi(\cdot) \tag{30}$$

$$\varepsilon_3 \dot{\eta} = A_\eta \eta + \varepsilon_3 \left[\bar{B}_1 \Delta_1 + \bar{B}_2 \Delta_2 + \left(\frac{1}{\varepsilon_2}\right) \bar{B}_2 \Delta_3\right] \tag{31}$$

where A_η, $\bar{B}_1$ and $\bar{B}_2$ are given in Appendix and $z = [z_F, z_u]^T$ with

$$z_F = F - F^*, \qquad z_u = u - u^*.$$

With the variables F^* and u^*, the conditions $f_x(\theta_1 + \alpha_r, \theta_2, F^*) - u^* = 0$ and $f_\alpha(\theta_1 + \alpha_r, \theta_2, F^*) - v_d = 0$ in (23) hold, and $\psi(\cdot) = 0$ when $\eta = 0$, and $\phi(\cdot)$ is bounded uniformly in ε_2. The fast variables $\eta = [\eta_x, \eta_\alpha]^T$, $\eta_x = [\eta_{x_1}, \eta_{x_2}, \eta_{x_3}]^T$ and $\eta_\alpha = [\eta_{\alpha_1}, \eta_{\alpha_2}, \eta_{\alpha_3}]^T$ are defined by

$$\begin{aligned} \eta_{x_1} &= \frac{x_1 - \hat{x}_1}{\varepsilon_3^2}, \qquad \eta_{x_2} = \frac{x_2 - \hat{x}_2}{\varepsilon_3}, \\ \eta_{x_3} &= \sigma_x(\theta_1 + \alpha_r, \theta_2, F) - \hat{\sigma}_x \\ \eta_{\alpha_1} &= \frac{\alpha_1 - \hat{\alpha}_1}{\varepsilon_3^2}, \qquad \eta_{\alpha_2} = \frac{\alpha_2 - \hat{\alpha}_2}{\varepsilon_3}, \\ \eta_{\alpha_3} &= \sigma_\alpha(\theta_1 + \alpha_r, \theta_2, F) - \hat{\sigma}_\alpha. \end{aligned}$$

We note that f_x and f_α of (28) and (29) are bounded uniformly in ε_2 and ε_3.

The stability analysis for the each subsystem will be done by starting from the fastest one, i.e. the error dynamics of the two EHGOs (31) to the slowest one, i.e. the cart dynamics (28). The singularly perturbed system can be viewed as a two-time-scale structure if the error dynamics of the two EHGOs (31) are the fast subsystem, while other subsystems (28)–(30) are the slow one as depicted in Fig. 3. The boundary layer system, which is obtained by setting $\varepsilon_3 = 0$ in (31),

$$\varepsilon_3 \left(\frac{d\eta}{dt}\right) = A_\eta \eta$$

is exponentially stable. We note that in the error dynamics of the EHGOs, the matrix A_η is Hurwitz, and Δ_1, Δ_2, and Δ_3 and the constant matrix $\bar{B}_1$, $\bar{B}_2$, and $\bar{B}_3$ are uniformly bounded in ε_3 whose definitions are given in Appendix.

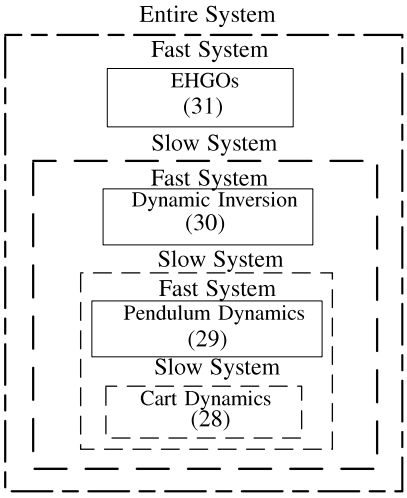

Fig. 3. Multi-time-scale structure for the closed-loop system.

Next, the dynamic inversion (30) is slow relative to the EHGOs and fast relative to the systems (28) and (29) as depicted in Fig. 3. Setting $\varepsilon_3 = 0$ and $\eta = 0$, which yields

$$x = \hat{x}, \qquad \alpha = \hat{\alpha}, \qquad f_x = \bar{f}_x + \hat{\sigma}_x, \qquad f_\alpha = \bar{f}_\alpha + \hat{\sigma}_\alpha,$$

results in the boundary layer system

$$\varepsilon_2 \dot{z} = A_z z + \begin{bmatrix} -f_x(\theta_1 + \alpha_r, \theta_2, F^*) + u^* \\ f_\alpha(\theta_1 + \alpha_r, \theta_2, F^*) - v_d \end{bmatrix} - \varepsilon_2 \begin{bmatrix} \dot{F}^* \\ \dot{u}^* \end{bmatrix}$$

with

$$\begin{aligned} f_x(\theta_1 + \alpha_r, \theta_2, F^*) &= c_x F^* + G_x, \\ f_\alpha(\theta_1 + \alpha_r, \theta_2, F^*) &= -c_\alpha F^* + G_\alpha. \end{aligned}$$

Since $f_x(\theta_1 + \alpha_r, \theta_2, F^*) - u^* = 0$ and $f_\alpha(\theta_1 + \alpha_r, \theta_2, F^*) - v_d = 0$ with the inputs F^* and u^*, we have

$$\varepsilon_2 \dot{z} = A_z z - \varepsilon_2 \begin{bmatrix} \dot{F}^* \\ \dot{u}^* \end{bmatrix}.$$

Setting $\varepsilon_2 = 0$ yields exponential stability of $z = 0$.

After the EHGOs and dynamic inversion reach quasi-steady state, hierarchically, i.e.,

$$\varepsilon_3 = 0, \qquad \eta = 0, \qquad \varepsilon_2 = 0, \qquad z = 0$$

we have the reduced system for the inverted pendulum on a cart which is the same as the system in (17). The reduced system also has a time-scale structure and its stability analysis is given in Section 2.4.

Typically, a slow variable in a multi-time-scale structure is assumed to be constant although it is evolving slowly. We consider the behavior of the slow variable and define sets for stability analysis of our multi-time-scale structure using Lyapunov functions. Lyapunov functions for three of the four subsystems are defined by; $V_y = y^T P_y y$, $V_z = z^T P_z z$, and $V_\eta = \eta^T P_\eta \eta$, where P_y, P_z, and P_η are solutions of Lyapunov equations with right-hand sides equal to the negative identity matrix. The Lyapunov function V_θ is defined in (21). The fastest variable η converges quickly into the set

$\{V_\eta \le \rho(\varepsilon_3/\varepsilon_2)^2\}$ with a positive constant ρ, while the variables y, θ, and z move relatively slowly. We define a set $(y,\theta,z) \in \{V_y \le a_1\} \times \{V_\theta \le a_2\} \times \{V_z \le a_3\}$ with positive constants a_1, a_2, and a_3. Although a short convergence time period $T_1(\varepsilon_3)$ exists for the fastest variable η, the trajectories of variables y, θ, and z can leave the set $\{V_y \le a_1\} \times \{V_\theta \le a_2\} \times \{V_z \le a_3\}$. Therefore, we define the superset $\{V_y \le b_1\} \times \{V_\theta \le b_2\} \times \{V_z \le b_3\}$, where b_i, $(b_i > a_i)$ can be arbitrarily close to a_i, $i = 1, 2, 3$, (for a sufficiently small ε_3) that satisfies the condition for the constrained domain for θ. After the variable η converges into the set $\{V_\eta \le \rho(\varepsilon_3/\varepsilon_2)^2\}$, we consider the time period $T_2(\varepsilon_2)$ for convergence of the second fastest variable z. During the time period $T_2(\varepsilon_2)$, the trajectories of y and θ can leave the set $\{V_y \le b_1\} \times \{V_\theta \le b_2\}$. To guarantee that the condition for the constrained domain for θ is satisfied during both time periods $T_1(\varepsilon_3)$ and $T_2(\varepsilon_2)$, we define the superset $(y,\theta) \in \{V_y \le A_1\} \times \{V_\theta \le A_2\}$ where A_i $(A_i > b_i)$ can be arbitrarily close to b_i, $i = 1, 2$, (for a sufficiently small ε_2).

The main result of this paper is presented next with the help of the following theorem.

Theorem 1. *Let X_1 be any compact set of (x,α) in the domain $D_x \times D_\alpha$, X_2 any compact subset of $\mathbf{R}^2$, and X_3 any compact subset of $\mathbf{R}^6$. There exists ε^* such that for all*

$$\varepsilon_1 < \varepsilon^*, \qquad \varepsilon_2 < \varepsilon^*, \qquad \frac{\varepsilon_3}{\varepsilon_2} < \varepsilon^*, \qquad \varepsilon_3 < \varepsilon^*$$

and for all initial states $(x(0),\alpha(0)) \in X_1$, $(F(0),u(0)) \in X_2$, and $(\hat{x}(0),\hat{\alpha}(0)) \in X_3$, the closed-loop system (28)–(31) has an exponentially stable equilibrium point, at which $x = 0$ and $\alpha = 0$, and the set $X_1 \times X_2 \times X_3$ is a subset of the region of attraction.

Proof. It is shown in Appendix that the closed-loop system (28)–(31) can be written as

$$\dot{y} = \varepsilon_1 \left[A_y y + B\big(h_x(\theta,\alpha_r) + c_x z_F\big)\right] \tag{32}$$

$$\dot{\theta} = A_\theta \theta + \varepsilon_1 E h_\alpha(y,\theta,\alpha_r,F) - B c_\alpha z_F \tag{33}$$

$$\varepsilon_2 \dot{z} = A_z z + \psi(\cdot) - \varepsilon_2 \phi(\cdot) \tag{34}$$

$$\varepsilon_3 \dot{\eta} = A_\eta \eta + \varepsilon_3 \left[\bar{B}_1 \Delta_1 + \bar{B}_2 \Delta_2 + \left(\frac{1}{\varepsilon_2}\right) \bar{B}_2 \Delta_3\right]. \tag{35}$$

For the first part of the proof, all trajectories starting from $(x(0),\alpha(0),F(0),u(0)) \in X_1 \times X_2$, will converge into the desired equilibrium while α_1 satisfies the condition for the constrained domain. We are going to show that all trajectories converge to a positive invariant set $\{V_y \le d_1\} \times \{V_\theta \le (\varepsilon_\theta^*)^2 d_2\} \times \{V_z \le (\varepsilon_z^*)^2 c_3\} \times \{V_\eta \le (\varepsilon_3/\varepsilon_2)^2 \rho\}$ with the positive constants d_1, d_2, c_3, ρ, $\varepsilon_\theta^* = \max\{\varepsilon_1, \varepsilon_z^*\}$, and $\varepsilon_z^* = \max\{\varepsilon_2, (\varepsilon_3/\varepsilon_2)\}$. Note that it is shown that in Section 2.4, the condition for the constrained domain for α_1 with sufficiently small $\varepsilon_1 > 0$, is satisfied even though change of variables is used. We are going to use the following hierarchical, repeated process

- First, we are going to prove that a subset $\{V_z \le b_3\} \times \{V_\eta \le (\varepsilon_3/\varepsilon_2)^2 \rho\}$ of $\{V_y \le b_1\} \times \{V_\theta \le b_2\} \times \{V_z \le b_3\} \times \{V_\eta \le (\varepsilon_3/\varepsilon_2)^2 \rho\}$ is positively invariant by properly choosing ρ, while the variable η is viewed as fast and the other variables y, θ, and z are considered as slow. The time period $T_1(\varepsilon_3)$ for η to converge into the set $\{V_\eta \le (\varepsilon_3/\varepsilon_2)^2 \rho\}$, can be arbitrarily small as $\varepsilon_3 \to 0$.
- Second, it will be shown that the subset $\{V_\theta \le c_2\} \times \{V_z \le (\varepsilon_z^*)^2 c_3\} \times \{V_\eta \le (\varepsilon_3/\varepsilon_2)^2 \rho\}$ of $\{V_y \le c_1\} \times \{V_\theta \le c_2\} \times \{V_z \le (\varepsilon_z^*)^2 c_3\} \times \{V_\eta \le (\varepsilon_3/\varepsilon_2)^2 \rho\}$ with $b_1 < c_1 < A_1$ and $b_2 < c_2 < A_2$ is positively invariant by properly choosing c_3. In this stage, the variable η is already in the set $\{V_\eta \le (\varepsilon_3/\varepsilon_2)^2 \rho\}$ and the variable z converges rapidly into the set $\{V_z \le (\varepsilon_z^*)^2 c_3\}$ with the convergence time period $T_2(\varepsilon_2)$. The time $T_2(\varepsilon_2)$ can be arbitrarily small as $\varepsilon_2 \to 0$.
- Lastly, it will be claimed that the set of $\{V_y \le d_1\} \times \{V_\theta \le (\varepsilon_\theta^*)^2 d_2\} \times \{V_z \le (\varepsilon_z^*)^2 c_3\} \times \{V_\eta \le (\varepsilon_3/\varepsilon_2)^2 \rho\}$ with $c_1 < d_1 < A_1$ is positively invariant by properly choosing d_2. In this stage, the variables z and η are in the set $\{V_z \le (\varepsilon_z^*)^2 c_3\} \times \{V_\eta \le (\varepsilon_3/\varepsilon_2)^2 \rho\}$ and the fast variable θ converges into $\{V_\theta \le (\varepsilon_\theta^*)^2 d_2\}$.

In this proof, we are going to show only the first bullet out of three since proofs for the others are the same as the first bullet. There is an upper bound $\|\eta\| \le (\varepsilon_3/\varepsilon_2)\sqrt{\rho/\lambda_{\min}(P_\eta)}$, where symbols $\lambda_{\max}(N)$ and $\lambda_{\min}(N)$ are used to denote maximum and minimum eigenvalues of a matrix N, respectively, and the variables y and θ are in a compact set. The derivative of V_z along the trajectory (34) is

$$\begin{aligned}\dot{V}_z \le & -\left(\frac{1}{\varepsilon_2}\right)\|z\|^2 + \left(\frac{2}{\varepsilon_2}\right) P_{z_m} k_\psi \|\eta\|\,\|z\| \\ & + 2P_{z_m}\Big[k_{\phi_1}\|y\| + k_{\phi_2}\|\theta\| + k_{\phi_3}\|z\|\Big]\|z\| \le -\frac{a_z}{2\varepsilon_2}\|z\|^2 \\ & \text{for } \|z\| \ge \varepsilon_z^* \left(\frac{4P_{z_m}}{a_z}\right) k_{z_b}\end{aligned} \tag{36}$$

for all $(y,\theta,z,\eta) \in \{V_y \le b_1\} \times \{V_\theta \le b_2\} \times \{V_z = b_3\} \times \{V_\eta \le (\varepsilon_3/\varepsilon_2)^2 \rho\}$, where $a_z = 1 - 2\varepsilon_2 k_{\phi_1} P_{z_m}$, $P_{z_m} = \lambda_{\max}(P_z)$, and the positive constants k_{z_b}, k_ψ, k_{ϕ_1}, k_{ϕ_2}, and k_{ϕ_3} are independent of ε_z^*. The derivative of V_η along the trajectory (35) is

$$\begin{aligned}\dot{V}_\eta \le & -\frac{1}{\varepsilon_3}\|\eta\|^2 + 2P_{\eta_m}\Bigg[(k_{\eta_1}\|y\| + k_{\eta_2}\|\theta\| + k_{\eta_3}\|z\|) \\ & + \left(\frac{1}{\varepsilon_2}\right)(k_{\eta_4}\|z\| + k_{\eta_5}\|\eta\|) + k_{\eta_6}\|\eta\|\Bigg]\|\eta\| \\ \dot{V}_\eta \le & -\frac{a_\eta}{2\varepsilon_3}\|\eta\|^2, \quad \text{for } \|\eta\| \ge \left(\frac{\varepsilon_3}{\varepsilon_2}\right)\left(\frac{4P_{\eta_m}}{a_\eta}\right) b_\eta\end{aligned} \tag{37}$$

for all $(y,\theta,z,\eta) \in \{V_y \le b_1\} \times \{V_\theta \le b_2\} \times \{V_z \le (\varepsilon_z^*)^2 b_3\} \times \{V_\eta = \rho(\varepsilon_3/\varepsilon_2)^2\}$, where $a_\eta = 1 - 2P_{\eta_m}\big[(\varepsilon_3/\varepsilon_2)k_{\eta_5} + \varepsilon_3 k_{\eta_6}\big]$, $P_{\eta_m} = \lambda_{\max}(P_\eta)$, and the positive constants b_η and k_{η_1} to k_{η_6} are independent of $(\varepsilon_3/\varepsilon_2)$. By choosing $\rho = 16P_{\eta_m}^3 (b_\eta/a_\eta)^2$ and using (36) and (37), we conclude that the set $\{V_z \le b_3\} \times \{V_\eta \le (\varepsilon_3/\varepsilon_2)^2 \rho\}$ is positively invariant.

Now, it will be shown that for sufficiently small ε_3, trajectories starting from $(F,u) \in X_2$ and $(\hat{x},\hat{\alpha}) \in X_3$ enter the corresponding invariant set of $\{V_z \le b_3\} \times \{V_\eta \le \rho(\varepsilon_3/\varepsilon_2)^2\}$ in the finite time $T_1(\varepsilon_3)$, where $\lim_{\varepsilon_3 \to 0} T_1(\varepsilon_3) = 0$. There exists the error bound $\|\eta(0)\| \le k_t/\varepsilon_3^2$ with a non-negative constant k_t. Due to the continuity and boundedness of $\dot{y}$, $\dot{\theta}$, and $\dot{z}$, we have

$$\|y(t) - y(0)\| \le k_f t, \qquad \|\theta(t) - \theta(0)\| \le k_f t,$$
$$\|z(t) - z(0)\| \le k_f t$$

with the constant $k_f > 0$. Instead of computing the time T_n when the trajectory η enters into the set $\{V_\eta \le \rho(\varepsilon_3/\varepsilon_2)^2\}$, we will find the longer time T_1 than T_n to ensure that the trajectory enters the set in a finite time. Using the bound for the initial condition of η and the property of exponential stable Lyapunov function V_η in (37), we have

$$V_\eta \le \left(\frac{\sigma_2}{\varepsilon_3^4}\right) \exp(-\sigma_1 t/\varepsilon_3)$$

where $\sigma_1 = a_\eta/(2P_{\eta_m})$ and $\sigma_2 = P_{\eta_m}k_t^2$. Due to $\varepsilon_3 < (\varepsilon_3/\varepsilon_2)$, we obtain

$$\varepsilon_3^2\rho = \left(\frac{\sigma_2}{\varepsilon_3^4}\right)\exp(-\sigma_1 T_1/\varepsilon_3).$$

The bound for the time $T_1(\varepsilon_3) \in (0, T_0]$ is obtained

$$T_1(\varepsilon_3) = \left(\frac{\varepsilon_3}{\sigma_1}\right)\ln\left(\frac{\sigma_2}{\rho_4\varepsilon_3^6}\right) \le \frac{1}{2}T_0.$$

As $\varepsilon_3 \to 0$, $T_1(\varepsilon_3) \to 0$.

As the second part of the proof, we are going to show that the closed-loop system (28)–(31) has an exponentially stable equilibrium point, at which $x = 0, \alpha = 0$. Consider the derivative of the Lyapunov functions V_θ and V_z along the trajectories (33) and (34), respectively, are

$$\dot V_\theta \le -k_m\|\theta\|^2 + \Big[\varepsilon_1 k_{h_1}\|y\| + \varepsilon_1 k_{h_2}\|\theta\| + \left(\varepsilon_1 k_{h_3} + c_{\alpha_m}\right)\|z\|\Big]\|\theta\| \tag{38}$$

$$\dot V_y \le \varepsilon_1[-\|y\|^2 + 2k_\theta P_{y_m}\|\theta\|\,\|y\| + 2c_{x_m}P_{y_m}\|z\|\,\|y\|] \tag{39}$$

where $P_{y_m} = \lambda_{\max}(P_y)$, $\|c_x\| \le c_{x_m}$, $\|c_\alpha\| \le c_{\alpha_m}$ and the positive constants k_m, k_{h_1}, k_{h_2}, k_{h_3}, and k_θ are independent of ε_1, ε_2, ε_3, and $(\varepsilon_3/\varepsilon_2)$.

By defining $W_y = \sqrt{V_y}$, $W_\theta = \sqrt{V_\theta}$, $W_z = \sqrt{V_z}$, and $W_\eta = \sqrt{V_\eta}$ and using (36)–(39), we have

$$D^+W \le -MW, \quad W = [W_y, W_\theta, W_z, W_\eta]^T$$

$$M = \begin{bmatrix} \varepsilon_1 k_{11} & -\varepsilon_1 k_{12} & -\varepsilon_1 k_{13} & 0 \\ -\varepsilon_1 k_{21} & (1-\varepsilon_1 k_{22})k_{22}^* & -(\varepsilon_1 k_{23} + k_{23}^*) & 0 \\ -k_{31} & -k_{32} & \left(\frac{k_{33}}{\varepsilon_2}\right)(1-\varepsilon_2 k_{33}^*) & -\frac{k_{34}}{\varepsilon_2} \\ -k_{41} & -k_{42} & -\left(k_{43} + \frac{k_{43}^*}{\varepsilon_2}\right) & k_M \end{bmatrix}$$

where $k_M = \frac{1}{\varepsilon_3}\left(1 - \varepsilon_3 k_{44} - \frac{\varepsilon_3}{\varepsilon_2}k_{44}^*\right)$ and $D^+W(\cdot)$ denotes the upper right-hand derivative, and k_{ij} and k_{ij}^* for $i, j = 1, \ldots, 4$ are positive constants independent of ε_1, ε_2, ε_3, and $(\varepsilon_3/\varepsilon_2)$. Consider the differential equation $\dot U = -MU$ with $U = [U_y, U_\theta, U_z, U_\eta]^T$ and the same initial condition $U(0) = W(0)$, whose origin is exponentially stable since the leading principal minors of the matrix M can be all positive (i.e., the matrix M can be Hurwitz) by choosing $\varepsilon_1 \ll 1$, $\varepsilon_2 \ll 1$, $\varepsilon_3 \ll 1$, and $\varepsilon_3/\varepsilon_2 \ll 1$ small enough. Using a vectorial comparison method in Chapter IX of Rouche, Habets, and Laloy (1977), we conclude that $W \le U$ for all $t \ge 0$. Therefore, the closed-loop system (28)–(31) has an exponentially stable equilibrium point, at which $x = 0, \alpha = 0$. □

4. Simulation and experiment

4.1. Simulation results

For simulations, the system parameters were assumed to be

$$m_c = 0.94\text{ kg}, \quad m_p = 0.23\text{ kg}$$
$$g = 9.8\text{ m/s}^2, \quad \ell = 0.3206\text{ m}. \tag{40}$$

The state feedback controller described by (4), (5), (10), and (12) was implemented using the following parameter values; The control parameters for the state feedback are

$$\gamma_1 = \varepsilon_1^2 k_1, \quad \gamma_2 = \varepsilon_1 k_2, \quad \beta_1 = 5, \quad \beta_2 = 3 \tag{41}$$

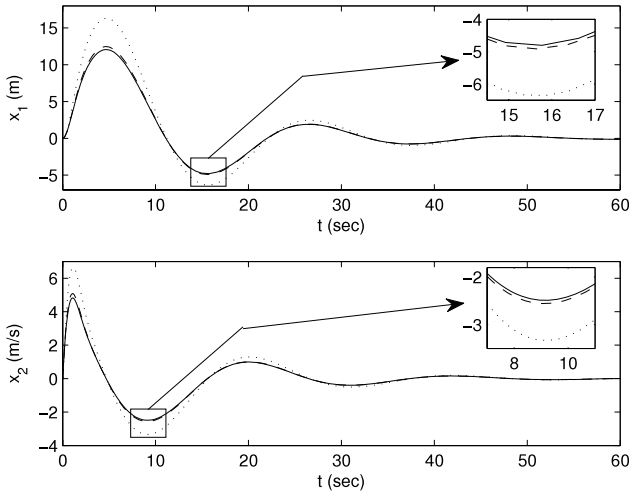

Fig. 4. Trajectories of x_1 and x_2 for state feedback (solid line), output feedback with $(\varepsilon_2, \varepsilon_3) = (0.02, 0.002)$ (dotted line), and output feedback with $(\varepsilon_2, \varepsilon_3) = (0.01, 0.0001)$ (dashed line).

where ε_1, k_1, and k_2 were chosen as

$$\varepsilon_1 = 0.2, \quad k_1 = 2, \quad k_2 = 1. \tag{42}$$

For the output feedback controller, we assume that the system dynamics is completely unknown except for the sign conditions in (22). The output feedback controller with dynamic inversion described by (25)–(27) was implemented by setting $\bar f_x(\cdot) = 0$ and $\bar f_\alpha(\cdot) = 0$ in (25) and (26). The following parameter values were used

$$h_{i1} = 5, \quad h_{i2} = 5, \quad h_{i3} = 4, \quad i = 1, 2.$$

The parameters ε_1 and β_i, γ_i, $i = 1, 2$, are the same as those used in state feedback control—see (41) and (42). The saturation limits M_x, M_α, and M_θ are chosen to be slightly greater than the maximum absolute values of f_x, f_α, and α_2, respectively, observed in state feedback control simulations. For both state feedback and output feedback, the initial states $x_1(0)$, $x_2(0)$, $\alpha_1(0)$, and $\alpha_2(0)$ were chosen as

$$x_1(0) = 0\text{ m}, \quad x_2(0) = 0\text{ m/s},$$
$$\alpha_1(0) = 0.8727\text{ rad } (50^\circ), \quad \alpha_2(0) = 0\text{ rad/s}.$$

The initial conditions used for the dynamic inversion and the EHGOs were

$$F(0) = 0, \quad u(0) = 0,$$
$$\hat x_1(0) = 0.1, \quad \hat x_2(0) = 0.1, \quad \hat f_x(0) = 0,$$
$$\hat\alpha_1(0) = 0.1, \quad \hat\alpha_2(0) = 0.1, \quad \hat f_\alpha(0) = 0.$$

To investigate the performance of output feedback vis-a-vis state feedback, we simulate two cases with: $(\varepsilon_2, \varepsilon_3) = (0.02, 0.002)$ and $(\varepsilon_2, \varepsilon_3) = (0.01, 0.0001)$. The results are shown in Figs. 4 and 5.

The plots of x_1 and x_2 are shown in Fig. 4 and the plots of α_1 and α_2 are shown in Fig. 5; these plots have different time horizons since the dynamics of x_1 and x_2 are slower than the dynamics of α_1 and α_2. Both Figs. 4 and 5 indicate that the states converge to the desired values and the output feedback controller is able to recover the performance of the state feedback controller when ε_2 and ε_3 are chosen small enough.

We present results from a second simulation where the initial configuration of the pendulum is almost horizontal with different initial conditions. The initial conditions were assumed to be

$$x_1(0) = 0\text{ m}, \quad x_2(0) = -3\text{ m/s},$$
$$\alpha_1(0) = 1.3963\text{ rad } (80^\circ), \quad \alpha_2(0) = \frac{\pi}{2}\text{ rad/s}.$$

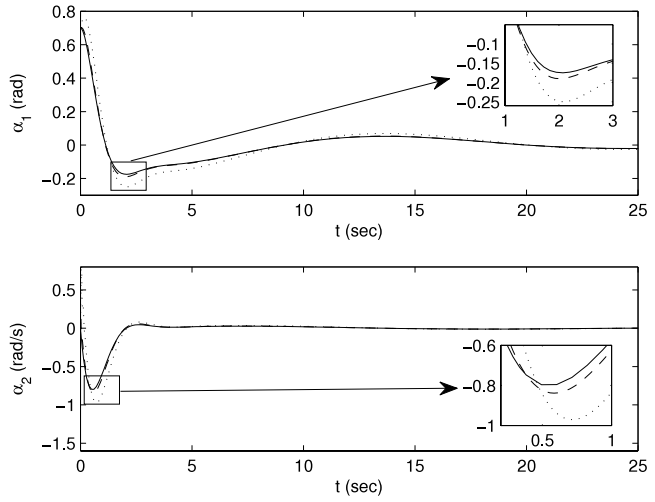

Fig. 5. Trajectories of α_1 and α_2 for state feedback (solid line), output feedback with $(\varepsilon_2, \varepsilon_3) = (0.02, 0.002)$ (dotted line), and output feedback with $(\varepsilon_2, \varepsilon_3) = (0.01, 0.0001)$ (dashed line).

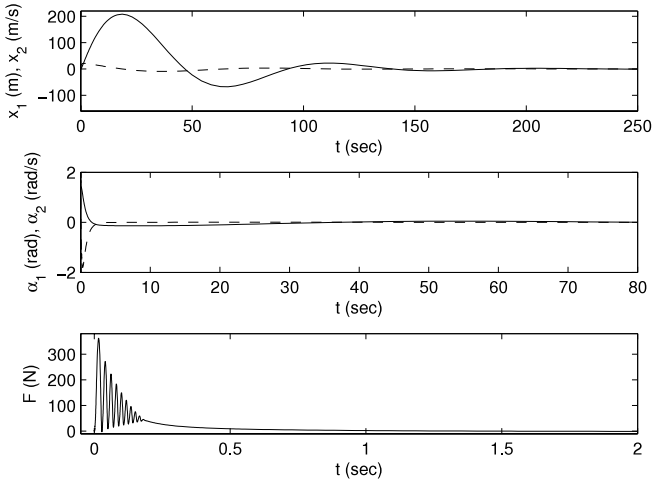

Fig. 6. Trajectories of x_1 and α_1 (solid lines), and x_2 and α_2 (dashed lines) are shown in the top and middle subfigures. In the bottom subfigure, a trajectory of the input F in (26) is shown.

The time-scale control parameters ε_1, ε_2, and ε_3 were chosen as $\varepsilon_1 = 0.05$, $\varepsilon_2 = 0.002$ and $\varepsilon_3 = 0.0001$, and the control parameters β_1 and β_2 were chosen as $\beta_1 = 15$, $\beta_2 = 10$. The remaining control parameters and initial conditions were chosen to be identical to the first simulation. The results, shown in Fig. 6, indicate that the pendulum and the cart are both successfully stabilized to their desired configuration.

4.2. Experimental results

The experimental testbed for the inverted pendulum on a cart is shown in Fig. 7. A 6V-DC motor with a planetary gearhead (reduction ratio 3.71:1) drives the cart on the racks. The angle of the pendulum and the position of the cart are measured by optical encoders that have a resolution of 1024 lines per revolution. The experimental hardware was interfaced with a dSPACE board and the output feedback controller was implemented in the Matlab/Simulink environment with a sampling interval of 0.0006 s.

The dynamics of the inverted pendulum on a cart is described by (2) and (3) and the nominal parameter values are given by (40). The dynamic inversion based output feedback controller described by

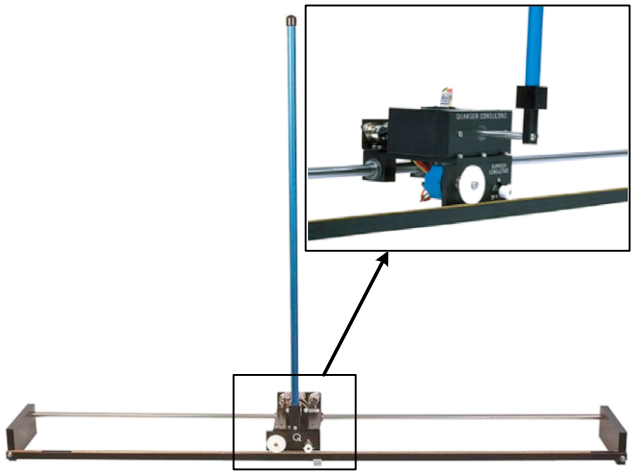

Fig. 7. Experimental testbed for the inverted pendulum on a cart—a product of Quanser (http://www.quanser.com/Products/linear_servo_IP02).

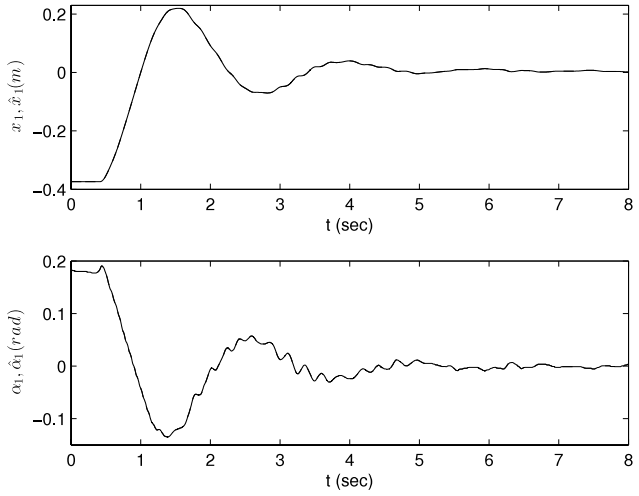

Fig. 8. Trajectories of x_1 and its estimate $\hat{x}_1$, and α_1 and its estimate $\hat{\alpha}_1$ are shown. The estimated values are indistinguishable from their true (measured) values.

(25)–(27) was implemented using the following parameter values

$$k_1 = 9, \quad k_2 = 5, \quad \gamma_1 = \varepsilon_1^2 k_1, \quad \gamma_2 = \varepsilon_1 k_2,$$
$$\beta_1 = 50, \quad \beta_2 = 30,$$
$$h_{i1} = 3, \quad h_{i2} = 3, \quad h_{i3} = 1, \quad \text{for } i = 1, 2$$
$$\varepsilon_1 = 0.2, \quad \varepsilon_2 = 0.01, \quad \varepsilon_3 = 0.005.$$

The initial conditions were chosen as follows:

$$x_1(0) = -0.38 \text{ m}, \quad x_2(0) = 0 \text{ m/s},$$
$$\alpha_1(0) = 0.19 \text{ rad } (10.9^\circ), \quad \alpha_2(0) = 0 \text{ rad/s}.$$

The initial angle of the pendulum was chosen close to the upright configuration such that the cart position did not exceed the physical limit of the racks and the motor did not exceed its torque limit. To reduce the effect of measurement noise, the encoder signals were passed through low-pass filters of bandwidth 1000 Hz.

The experimental results are shown in Fig. 8. Until around 0.5 s, the pendulum on the cart is held manually while the power switch is off. At around 0.5 s, the power switch is turned on. The trajectories of x_1 and its estimate $\hat{x}_1$, and α_1 and its estimate $\hat{\alpha}_1$, all converge to the origin.

Within an allowable operation range of the system, we compared experimentally results generated by our control algorithm

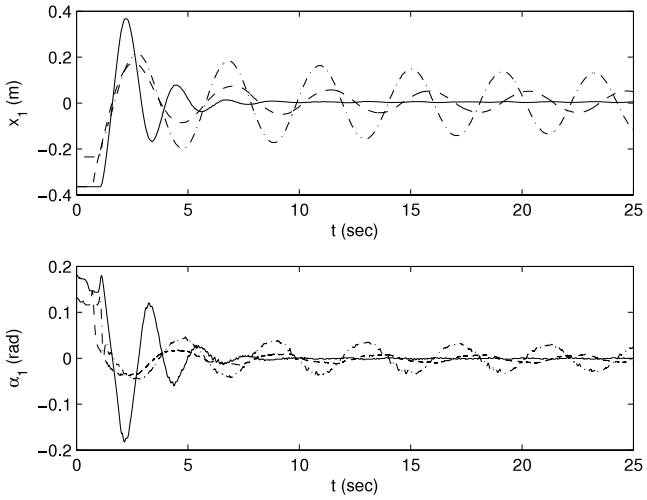

Fig. 9. Trajectories of x_1 and α_1 are shown with different control schemes. Solid lines driven by our control scheme, converge into the origin. Dotted lines generated by an LQR controller, have ultimate boundedness. Dash–dot lines provided by the control algorithm in Srinivasan et al. (2009) have the biggest ultimate boundedness.

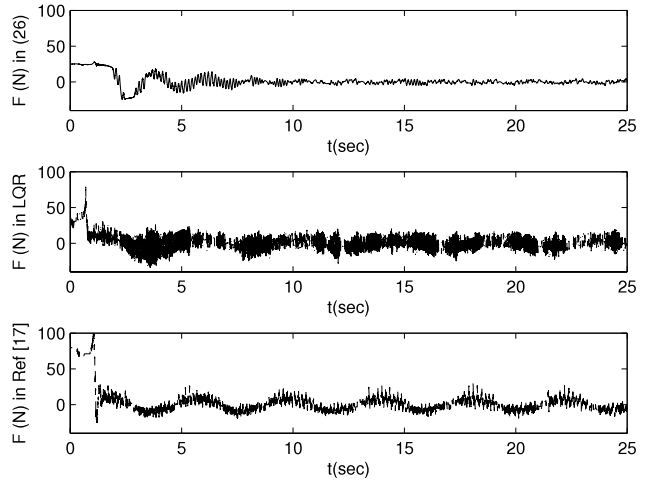

Fig. 10. Trajectories of inputs F in (26) (the top subfigure), LQR (the middle subfigure), and Srinivasan et al. (2009) (the bottom subfigure) are shown.

with ones provided by an LQR controller and the control algorithm in Srinivasan et al. (2009). The LQR controller is designed by following instructions in manufacturer manuals. The stabilization control scheme proposed by Srinivasan et al. (2009) was also implemented to check the effectiveness of estimates of uncertainties by the EHGOs. In Fig. 9, we show the ultimate boundedness results from system uncertainties, which could be due to friction between cart's pion and racks, mass of the cart and pendulum, etc. In Fig. 10, the effectiveness of fast estimates by the EHGOs with the dynamic inversion results in the appropriate control input F whereas the other two controllers use high gains to stabilize the system at the equilibrium in the presence of uncertainties.

5. Conclusion

An output feedback controller for stabilization of an inverted pendulum on a cart was presented. From a practical point of view, this is an important contribution since all states of the system are typically not accessible and uncertainties reside in the system. To estimate the unmeasured states and to compensate for the uncertain dynamics, Extended High-Gain Observers were used. To deal with uncertainties in the input coefficients, dynamic inversion was used. Both Extended High-Gain Observers and dynamic inversion introduce fast time scales and this required the controller to be designed using a multi-time-scale structure. The multi-time-scale structure is well-suited for control of underactuated systems, and for the inverted pendulum on a cart, additional time scale separation was used to first converge the pendulum to a reference trajectory and then converge the cart to its desired configuration. Using singular perturbation methods, the stability of the closed-loop system was analyzed and exponential stability of the equilibrium was established. Numerical simulations were used to show that the output feedback controller recovers the performance of state feedback and to demonstrate a large region of attraction of the equilibrium. Experimental results were used to demonstrate the feasibility of practical implementation with uncertainties in system parameters. Our future work will focus on extending our approach to output feedback stabilization of other underactuated mechanical systems.

Appendix

In this section, we are going to derive the standard singularly perturbed systems (32)–(35) with time-scaled variables.

A.1. Error dynamics of the EHGOs

With the fast variables for EHGOs are

$$\eta_{x_1} = \frac{x_1 - \hat{x}_1}{\varepsilon_3^2}, \qquad \eta_{x_2} = \frac{x_2 - \hat{x}_2}{\varepsilon_3},$$
$$\eta_{x_3} = \sigma_x(\theta_1 + \alpha_r, \theta_2, F) - \hat{\sigma}_x$$
$$\eta_{\alpha_1} = \frac{\alpha_1 - \hat{\alpha}_1}{\varepsilon_3^2}, \qquad \eta_{\alpha_2} = \frac{\alpha_2 - \hat{\alpha}_2}{\varepsilon_3},$$
$$\eta_{\alpha_3} = \sigma_\alpha(\theta_1 + \alpha_r, \theta_2, F) - \hat{\sigma}_\alpha,$$

with $\theta_1 = \alpha_1 - \alpha_r$, $\theta_2 = \alpha_2$, where $\hat{x}_i$ and $\hat{\alpha}_i$ for $i = 1, 2$, and $\hat{\sigma}_x$ and $\hat{\sigma}_\alpha$, are given in (25). The derivatives of η_{x_1} and η_{α_1} along the trajectories of (2) and (25) are

$$\varepsilon_3\dot{\eta}_{x_1} = -h_{11}\eta_{x_1} + \eta_{x_2}$$
$$\varepsilon_3\dot{\eta}_{\alpha_1} = -h_{21}\eta_{\alpha_1} + \eta_{\alpha_2}.$$

The derivatives of η_{x_2} and η_{α_2} along the trajectories of (2) and (25) are

$$\begin{aligned}\varepsilon_3\dot{\eta}_{x_2} &= -h_{12}\eta_{x_1} + \sigma_x(\alpha_1, \alpha_2, F) - \hat{\sigma}_x(t) \\ &\quad + \bar{f}_x(\alpha_1, \alpha_2, F) - \bar{f}_x(\hat{\alpha}_1, \hat{\alpha}_2, F) \\ &= -h_{12}\eta_{x_1} + \eta_{x_3} + \bar{f}_x(\alpha_1, \alpha_2, F) - \bar{f}_x(\hat{\alpha}_1, \hat{\alpha}_2, F) \\ \varepsilon_3\dot{\eta}_{\alpha_2} &= -h_{22}\eta_{\alpha_1} + \sigma_\alpha(\alpha_1, \alpha_2, F) - \hat{\sigma}_\alpha(t) \\ &\quad + \bar{f}_\alpha(\alpha_1, \alpha_2, F) - \bar{f}_\alpha(\hat{\alpha}_1, \hat{\alpha}_2, F) \\ &= -h_{22}\eta_{\alpha_1} + \eta_{\alpha_3} + \bar{f}_\alpha(\alpha_1, \alpha_2, F) - \bar{f}_\alpha(\hat{\alpha}_1, \hat{\alpha}_2, F).\end{aligned}$$

The derivatives of η_{x_3} and η_{α_3} along the trajectories of (2), (25) and (26) are

$$\begin{aligned}\varepsilon_3\dot{\eta}_{x_3} &= -h_{13}\eta_{x_1} + \varepsilon_3\dot{\sigma}_x(\alpha_1, \alpha_2, F) \\ &= -h_{13}\eta_{x_1} + \varepsilon_3 \left\{ \left(\frac{\partial \sigma_x}{\partial \alpha_1}\right)\alpha_2 + \left(\frac{\partial \sigma_x}{\partial \alpha_2}\right)\dot{\alpha}_2 \right. \\ &\quad - \frac{1}{\varepsilon_2} \cdot \left(\frac{\partial \sigma_x}{\partial F}\right) \left[\bar{f}_x\left(\alpha_1, M_\theta \mathrm{sat}\left(\frac{\hat{\alpha}_2}{M_\theta}\right), F\right) \right. \\ &\quad \left. \left. + M_x \mathrm{sat}(\hat{\sigma}_x/M_x) - u \right] \right\}\end{aligned}$$

$$\begin{aligned}\varepsilon_3\dot{\eta}_{\alpha_3} &= -h_{23}\eta_{\alpha_1} + \varepsilon_3\dot{\sigma}_\alpha(\alpha_1,\alpha_2,F)\\ &= -h_{23}\eta_{\alpha_1} + \varepsilon_3\left\{\left(\frac{\partial\sigma_\alpha}{\partial\alpha_1}\right)\alpha_2 + \left(\frac{\partial\sigma_\alpha}{\partial\alpha_2}\right)\dot{\alpha}_2\right.\\ &\quad -\frac{1}{\varepsilon_2}\cdot\left(\frac{\partial\sigma_\alpha}{\partial F}\right)\left[\bar{f}_x\left(\alpha_1, M_\theta\,\mathrm{sat}\left(\frac{\hat{\alpha}_2}{M_\theta}\right), F\right)\right.\\ &\quad \left.\left.+M_x\,\mathrm{sat}(\hat{\sigma}_x/M_x) - u\right]\right\}.\end{aligned}$$

The error dynamics for the EHGOs are

$$\varepsilon_3\dot{\eta} = A_\eta\eta + \varepsilon_3\left[\bar{B}_1\Delta_1 + \bar{B}_2\Delta_2 + \left(\frac{1}{\varepsilon_2}\right)\bar{B}_2\Delta_3\right]$$

where $\eta = [\eta_x^T, \eta_\alpha^T]^T$ with $\eta_x = [\eta_{x_1}, \eta_{x_2}, \eta_{x_3}]^T$ and $\eta_\alpha = [\eta_{\alpha_1}, \eta_{\alpha_2}, \eta_{\alpha_3}]^T$; the matrices $A_\eta = \begin{bmatrix} A_{\eta_1} & 0_{3\times3} \\ 0_{3\times3} & A_{\eta_2}\end{bmatrix}$, $\bar{B}_1$ and $\bar{B}_2$ are given by

$$A_{\eta_1} = \begin{bmatrix}-h_{11} & 1 & 0\\ -h_{12} & 0 & 1\\ -h_{13} & 0 & 0\end{bmatrix}, \qquad A_{\eta_2} = \begin{bmatrix}-h_{21} & 1 & 0\\ -h_{22} & 0 & 1\\ -h_{23} & 0 & 0\end{bmatrix},$$

$$\bar{B}_j = \begin{bmatrix} B_j & 0_{3\times1}\\ 0_{3\times1} & B_j\end{bmatrix}, \quad \text{for } j = 1, 2$$

$$B_1 = [0, 1, 0]^T, \qquad B_2 = [0, 0, 1]^T$$

with the zero matrix $0_{i\times j} \in \mathbf{R}^{i\times j}$, $B = [0, 1]^T$; and Δ_i for $i = 1, 2, 3$ are

$$\Delta_1 = \begin{bmatrix}\dfrac{\bar{f}_x(\alpha_1,\alpha_2,F) - \bar{f}_x(\hat{\alpha}_1,\hat{\alpha}_2,F)}{\varepsilon_3}\\ \dfrac{\bar{f}_\alpha(\alpha_1,\alpha_2,F) - \bar{f}_\alpha(\hat{\alpha}_1,\hat{\alpha}_2,F)}{\varepsilon_3}\end{bmatrix}$$

$$\Delta_2 = \begin{bmatrix}\left(\dfrac{\partial\sigma_x}{\partial\alpha_1}\right)\alpha_2 + \left(\dfrac{\partial\sigma_x}{\partial\alpha_2}\right)f_\alpha(\alpha_1,\alpha_2,F)\\ \left(\dfrac{\partial\sigma_\alpha}{\partial\alpha_1}\right)\alpha_2 + \left(\dfrac{\partial\sigma_\alpha}{\partial\alpha_2}\right)f_\alpha(\alpha_1,\alpha_2,F)\end{bmatrix}$$

$$\Delta_3 = \begin{bmatrix}\left(\dfrac{\partial\sigma_x}{\partial F}\right)\left[\bar{f}_x\left(\alpha_1, M_\theta\,\mathrm{sat}\left(\dfrac{\hat{\alpha}_2}{M_\theta}\right), F\right) + M_x\,\mathrm{sat}\left(\dfrac{\hat{\sigma}_x}{M_x}\right) - u\right]\\ \left(\dfrac{\partial\sigma_\alpha}{\partial F}\right)\left[\bar{f}_x\left(\alpha_1, M_\theta\,\mathrm{sat}\left(\dfrac{\hat{\alpha}_2}{M_\theta}\right), F\right) + M_x\,\mathrm{sat}\left(\dfrac{\hat{\sigma}_x}{M_x}\right) - u\right]\end{bmatrix}$$

where $\|\Delta_1\| \le k_\Delta\|\eta\|$ with a positive constant k_Δ due to the Lipschitz conditions $\|f_x(\alpha_1,\alpha_2,F) - \bar{f}_x(\hat{\alpha}_1,\hat{\alpha}_2,F)\| \le \varepsilon_3 k_{\Delta_x}\|\eta\|$ and $\|\bar{f}_\alpha(\alpha_1,\alpha_2,F) - \bar{f}_\alpha(\hat{\alpha}_1,\hat{\alpha}_2,F)\| \le \varepsilon_3 k_{\Delta_\alpha}\|\eta\|$ with positive constants k_{Δ_x} and k_{Δ_α}.

A.2. Error dynamics of the dynamic inversion

With the change of variables for the dynamic inversion,

$$z_F = F - F^*, \qquad z_u = u - u^*$$

the derivative of z_F along the trajectories of (2), (25), and (26) with multiplication of ε_2, is

$$\begin{aligned}\varepsilon_2\dot{z}_F &= \varepsilon_2\dot{F} - \varepsilon_2\dot{F}^*\\ &= -\bar{f}_x\left(\alpha_1, M_\theta\,\mathrm{sat}\left(\frac{\hat{\alpha}_2}{M_\theta}\right), F\right) - M_x\,\mathrm{sat}\left(\frac{\hat{\sigma}_x}{M_x}\right) + u - \varepsilon_2\dot{F}^*.\end{aligned}$$

By adding and subtracting $\bar{f}_x(\alpha_1,\alpha_2,F) + \sigma_x(\alpha_1,\alpha_2,F)$ and adding $\bar{f}_x(\alpha_1,\alpha_2,F^*) + \sigma_x(\alpha_1,\alpha_2,F^*) - u^*$ (i.e., $\bar{f}_x(\alpha_1,\alpha_2,F^*) + \sigma_x(\alpha_1,\alpha_2,F^*) - u^* = 0$) to the right-hand side of $\varepsilon_2\dot{z}_F$, we obtain

$$\begin{aligned}\varepsilon_2\dot{z}_F &= -\bar{f}_x(\alpha_1,\alpha_2,F) - \sigma_x(\alpha_1,\alpha_2,F)\\ &\quad +\bar{f}_x(\alpha_1,\alpha_2,F^*) + \sigma_x(\alpha_1,\alpha_2,F^*)\\ &\quad +\bar{f}_x(\alpha_1,\alpha_2,F) - \bar{f}_x\left(\alpha_1, M_\theta\,\mathrm{sat}\left(\frac{\hat{\alpha}_2}{M_\theta}\right), F\right)\\ &\quad +\sigma_x(\alpha_1,\alpha_2,F) - M_x\,\mathrm{sat}\left(\frac{\hat{\sigma}_x}{M_x}\right) + u - u^* - \varepsilon_2\dot{F}^*.\end{aligned}$$

Since

$$\begin{aligned}&\bar{f}_x(\alpha_1,\alpha_2,F^*) + \sigma_x(\alpha_1,\alpha_2,F^*)\\ &\quad -\bar{f}_x(\alpha_1,\alpha_2,F) - \sigma_x(\alpha_1,\alpha_2,F) = -c_x z_F,\end{aligned}$$

it is simplified to

$$\begin{aligned}\varepsilon_2\dot{z}_F &= -c_x z_F + z_u + \bar{f}_x(\alpha_1,\alpha_2,F) - \bar{f}_x\left(\alpha_1, M_\theta\,\mathrm{sat}\left(\frac{\hat{\alpha}_2}{M_\theta}\right), F\right)\\ &\quad +\sigma_x(\alpha_1,\alpha_2,F) - M_x\,\mathrm{sat}\left(\frac{\hat{\sigma}_x}{M_x}\right) - \varepsilon_2\dot{F}^*. \qquad (A.1)\end{aligned}$$

Since $F^* = F^*(\alpha_1,\alpha_2,\nu_d)$ is

$$F^* = \frac{[u^* - G_x]}{c_x}, \quad u^* = g\tan\alpha_1 - \left(\frac{\ell}{\cos\alpha_1}\right)\nu_d, \qquad (A.2)$$

with c_x in (22), G_x in (3), and ν_d in (12), $\dot{F}^*$ is

$$\begin{aligned}\dot{F}^* &= \left(\frac{\partial F^*}{\partial\alpha_1}\right)\dot{\alpha}_1 + \left(\frac{\partial F^*}{\partial\alpha_2}\right)\dot{\alpha}_2 + \left(\frac{\partial F^*}{\partial\nu_d}\right)\dot{\nu}_d\\ &= F_1(\theta_1+\alpha_r,\theta_2,F^*) + \varepsilon_1 F_2(\theta_1+\alpha_r,\theta_2,y,F^*)\end{aligned}$$

where F_1 and F_2 are

$$\begin{aligned}F_1 &= \left(\frac{\partial F^*}{\partial\alpha_1} - \beta_1\frac{\partial F^*}{\partial\nu_d}\right)\alpha_2 + \left(\frac{\partial F^*}{\partial\alpha_2} - \beta_2\frac{\partial F^*}{\partial\nu_d}\right)f_\alpha(\cdot)\\ F_2 &= -\beta_1\left(\frac{\partial F^*}{\partial\nu_d}\right)\left(\frac{g}{g^2+v_{ext}^2}\right)[k_1 y_2 + k_2 f_x(\cdot)].\end{aligned}$$

By differentiating z_u and multiplying $\dot{z}_u$ by ε_2, we obtain

$$\begin{aligned}\varepsilon_2\dot{z}_u &= \varepsilon_2\dot{u} - \varepsilon_2\dot{u}^*\\ &= \bar{f}_\alpha\left(\alpha_1, M_\theta\,\mathrm{sat}\left(\frac{\hat{\alpha}_2}{M_\theta}\right), F\right) + M_\alpha\,\mathrm{sat}\left(\frac{\sigma_\alpha}{M_\alpha}\right) - \hat{\nu}_d - \varepsilon_2\dot{u}^*.\end{aligned}$$

With the similar procedure of the derivation for $\varepsilon_2\dot{z}_F$, adding and subtracting $\bar{f}_\alpha(\alpha_1,\alpha_2,F) + \sigma_\alpha(\alpha_1,\alpha_2,F)$ and subtracting $\bar{f}_\alpha(\alpha_1,\alpha_2,F^*) + \sigma_\alpha(\alpha_1,\alpha_2,F^*) - \nu_d$ (i.e., $\bar{f}_\alpha(\alpha_1,\alpha_2,F^*) + \sigma_\alpha(\alpha_1,\alpha_2,F^*) - \nu_d = 0$), we obtain

$$\begin{aligned}\varepsilon_3\dot{z}_u &= -c_\alpha z_F + \bar{f}_\alpha\left(\alpha_1, M_\theta\,\mathrm{sat}\left(\frac{\hat{\alpha}_2}{M_\theta}\right), F\right) - \bar{f}_\alpha(\alpha_1,\alpha_2,F)\\ &\quad +M_\alpha\,\mathrm{sat}\left(\frac{\hat{\sigma}_\alpha}{M_\alpha}\right) - \sigma_\alpha(\alpha_1,\alpha_2,F) + \nu_d - \hat{\nu}_d - \varepsilon_2\dot{u}^* \qquad (A.3)\end{aligned}$$

where

$$\nu_d - \hat{\nu}_d = -\beta_1(\alpha_r - \hat{\alpha}_r) - \beta_2\left[M_\theta\,\mathrm{sat}\left(\frac{\hat{\alpha}_2}{M_\theta}\right) - \alpha_2\right]$$

with $\hat{\alpha}_r$ in (27) and $u^* = u^*(\alpha_1,\nu_d)$ in (A.2), $\dot{u}^*$ is

$$\begin{aligned}\dot{u}^* &= \left(\frac{\partial u^*}{\partial\alpha_1}\right)\dot{\alpha}_1 + \left(\frac{\partial u^*}{\partial\nu_d}\right)\dot{\nu}_d\\ &= u_1(\theta_1+\alpha_r,\theta_2,F) + \varepsilon_1 u_2(\theta_1+\alpha_r,\theta_2,y,F)\\ u_1 &= \left(\frac{\partial u^*}{\partial\alpha_1} - \beta_1\frac{\partial u^*}{\partial\nu_d}\right)\alpha_2 - \beta_2\left(\frac{\partial u^*}{\partial\nu_d}\right)f_\alpha(\cdot)\\ u_2 &= -\beta_1\left(\frac{\partial u^*}{\partial\nu_d}\right)\left(\frac{g}{g^2+v_{ext}^2}\right)[k_1 y_2 + k_2 f_x(\cdot)].\end{aligned}$$

With (A.1) and (A.3), we obtain

$$\varepsilon_2\dot{z} = A_z z + \psi(\cdot) - \varepsilon_2\phi(\cdot)$$

where A_z is given in (24), $z = [z_F, z_u]^T$, $\phi = [\dot{F}^*, \dot{u}^*]^T$, $\psi = [\psi_1, \psi_2 + \nu_d - \hat{\nu}_d]^T$ is

$$\begin{aligned}\psi_1 &= \bar{f}_x(\alpha_1, \alpha_2, F) - \bar{f}_x\left(\alpha_1, M_\theta \text{sat}\left(\frac{\hat{\alpha}_2}{M_\theta}\right), F\right) \\ &\quad + \sigma_x(\alpha_1, \alpha_2, F) - M_x \text{sat}\left(\frac{\hat{\sigma}_x}{M_x}\right) \\ \psi_2 &= \bar{f}_\alpha\left(\alpha_1, M_\theta \text{sat}\left(\frac{\hat{\alpha}_2}{M_\theta}\right), F\right) - \bar{f}_\alpha(\alpha_1, \alpha_2, F) \\ &\quad + M_\alpha \text{sat}\left(\frac{\hat{\sigma}_\alpha}{M_\alpha}\right) - \sigma_\alpha(\alpha_1, \alpha_2, F)\end{aligned}$$

and $\psi(\cdot)|_{\eta=0} = 0$ and when saturation is not effective $\|\psi\| \leq k_\psi \|\eta\|$ with a positive constant k_ψ.

A.3. Error dynamics of the plant

The change of variables $\theta_1 = \alpha_1 - \alpha_r$ with α_r in (11) and $\theta_2 = \alpha_2$ for the pendulum dynamics, and $y_1 = \varepsilon_1^2 x_1$ and $y_2 = \varepsilon_1 x_2$ for the cart dynamics, is used. The derivative of θ_1 along the trajectories of (2), (25), and (26) is

$$\dot{\theta}_1 = \dot{\alpha}_1 - \dot{\alpha}_r = \theta_2 + \varepsilon_1 h_\alpha \tag{A.4}$$

with h_α in (18) and the derivative of θ_2 is

$$\dot{\theta}_2 = f_\alpha(\alpha_1, \alpha_2, F) = -c_\alpha F + G_\alpha$$

with c_α in (22) and G_α in (3). Adding and subtracting $f_\alpha(\alpha_1, \alpha_2, F^*) = -c_\alpha F^* + G_\alpha$ with F^* and u^* in (A.2), we obtain

$$\begin{aligned}\dot{\theta}_2 &= f_\alpha(\alpha_1, \alpha_2, F^*) + f_\alpha(\alpha_1, \alpha_2, F) - f_\alpha(\alpha_1, \alpha_2, F^*) \\ &= -c_\alpha F^* + G_\alpha + f_\alpha(\alpha_1, \alpha_2, F) - f_\alpha(\alpha_1, \alpha_2, F^*) \\ &= -\beta_1\theta_1 - \beta_2\theta_2 - c_\alpha z_F.\end{aligned} \tag{A.5}$$

With (A.4) and (A.5), the pendulum dynamics is

$$\dot{\theta} = A_\theta \theta + \varepsilon_1 E h_\alpha(y, \theta, \alpha_r, F) - B c_\alpha z_F$$

where A_θ is given in (19), $\theta = [\theta_1, \theta_2]^T$, $E = [1, 0]^T$, and $B = [0, 1]^T$. With the slow variables of $y_1 = \varepsilon_1^2 x_1$ and $y_2 = \varepsilon_1 x_2$ for the cart dynamics, the derivatives of y_1 and y_2 along the trajectories of (2), (25), and (26) are

$$\begin{aligned}\dot{y}_1 &= \varepsilon_1 y_2 \\ \dot{y}_2 &= \varepsilon_1 f_x(\alpha_1, \alpha_2, F).\end{aligned} \tag{A.6}$$

With F^* and u^* in (A.2), adding and subtracting $\varepsilon_1 f_x(\alpha_1, \alpha_2, F^*) = \varepsilon_1[c_x F^* + G_x]$ to $\dot{y}_2$, it is obtained

$$\begin{aligned}\dot{y}_2 &= \varepsilon_1[f_x(\alpha_1, \alpha_2, F^*) + f_x(\alpha_1, \alpha_2, F) - (\alpha_1, \alpha_2, F^*)] \\ &= \varepsilon_1[c_x F^* + G_x + c_x z_F] \\ &= \varepsilon_1[-k_1 y_1 - k_2 y_2 + h_x + c_x z_F]\end{aligned} \tag{A.7}$$

with $h_x(\theta, \alpha_r)$ in (18) and $h_x(0, \alpha_r) = 0$. With (A.6) and (A.7), we obtain

$$\dot{y} = \varepsilon_1 \left[A_y y + B\big(h_x(\theta, \alpha_r) + c_x z_F\big)\right]$$

where A_y is given in (20) and $y = [y_1, y_2]^T$.

References

Adhikary, N., & Mahanta, C. (2013). Integral backstepping sliding mode control for underactuated systems: Swing-up and stabilization of the cart-pendulum system. *ISA Transactions*, *58*, 870–880.

Angeli, D. (2001). Almost global stabilization of the inverted pendulum via continuous state feedback. *Automatica*, *37*, 1103–1108.

Astolfi, A., Karagiannis, D., & Ortega, R. (2007). *Nonlinear and adaptive control design and applications*. London: Springer-Verlag.

Astrom, K. J., & Furuta, K. (2000). Swinging up a pendulum by energy control. *Automatica*, *36*, 287–295.

Auckly, D., Kapitanski, L., & White, W. (2000). Control of nonlinear underactuated systems. *Communications on Pure and Applied Mathematics*, *53*, 354–369.

Bloch, A. M., Chang, D. E., Leonard, N. E., & Marsden, J. E. (2001). Controlled Lagrangians and the stabilization of mechanical systems II: Potential shaping. *IEEE Transactions on Automatic Control*, *46*(10), 1556–1571.

Bloch, A. M., Leonard, N. E., & Marsden, J. E. (2000). Controlled Lagrangians and the stabilization of mechanical systems I: The first matching theorem. *IEEE Transactions on Automatic Control*, *45*(12), 2253–2270.

Cao, W., & Xu, J. (2004). Nonlinear integral-type sliding surface for both matched and unmatched uncertain systems. *IEEE Transactions on Automatic Control*, *49*, 1355–1360.

Fradkov, A. L. (1996). Swinging control of nonlinear oscillations. *International Journal of Control*, *64*, 1189–1202.

Getz, N. H. (1995). *Dynamic inversion of nonlinear maps with applications to nonlinear control and robotics* (Ph.D. thesis). University of California at Berkeley.

Getz, N. H., & Hedrick, J. K. (1995). An internal equilibrium manifold method of tracking for nonlinear nonminimum phase systems. In *IEEE American control conference, June* (pp. 2241–2245).

Hovakimyan, N., Lavretsky, E., & Cao, C. (2008). Dynamic inversion for multivariable non-affine-in-control system via time-scale separation. *International Journal of Control*, *81*, 1960–1967.

Hovakimyan, N., Lavretsky, E., & Sasane, A. J. (2005). Dynamic inversion for nonaffine-in-control systems via time-scale separation: Part I. In *Proc. IEEE int. American control conference* (pp. 3542–3547).

Khalil, H. K. (2002). *Nonlinear systems*. Printice Hall.

Kokotovic, P., Khalil, H. K., & O'Reilly, J. (1986). *Singular perturbation methods in control analysis and design*. SIAM.

Lee, J., Mukherjee, R., & Khalil, H. (2012). Performance recovery under output feedback for input nonaffine nonlinear systems. In *IEEE conference on decision and control, December* (pp. 326–331).

Lozano, R., Fantoni, I., & Block, D. J. (2000). Stabilization of the inverted pendulum around its homoclinic orbit. *Systems & Control Letters*, *40*, 197–204.

Mazenc, F., & Praly, L. (1996). Adding integrations, saturated controls, and stabilization for feedforward systems. *IEEE Transactions on Automatic Control*, *41*, 1559–1578.

Muralidharan, V., Ravichandran, M. T., & Mahindrakar, A. D. (2009). Extending interconnection and damping assignment passivity-based control (IDA-PBC) to underactuated mechanical systems with nonholonomic pfaffian constraints: The mobile inverted pendulum robot. In *IEEE conference on decision and control and 28th Chinese control conference* (pp. 6305–6310).

Olfati-Saber, R. (2002). Normal forms for underactuated mechanical systems with symmetry. *IEEE Transactions on Automatic Control*, *47*, 305–308.

Ortega, R., Spong, M., Gomez-Estern, F., & Blankenstein, G. (2002). Stabilization of class of underactuated mechanical systems via interconnection and damping assignment. *IEEE Transactions on Automatic Control*, *47*(10), 1218–1233.

Park, M., & Chwa, D. (2009). Swing-up and stabilization control of inverted-pendulum systems via coupled sliding-mode control method. *IEEE Transactions on Industrial Electronics*, *56*, 3541–3555.

Ravichandran, M. T., & Mahindrakar, A. D. (2011). Robust stabilization of a class of underactuated mechanical systems using time scaling and Lyapunov redesign. *IEEE Transactions on Industrial Electronics*, *58*, 4299–4313.

Rouche, D., Habets, P., & Laloy, M. (1977). *Stability theory by Lyapunov's direct method*. New York: Springer-Verlag.

Sarras, I., Acosta, J. A., Ortega, R., & Mahindrakar, A. D. (2013). Constructive immersion and invariance stabilization for a class of underactuated mechanical systems. *Automatica*, *49*, 1442–1448.

Shiriaev, A. S., Egeland, O., Ludvigsen, H., & Fradkov, A. L. (2001). Vss-version of energy-based control for swinging up a pendulum. *Systems & Control Letters*, *44*, 45–56.

Spong, M. W., & Praly, L. (1996). Control of underactuated mechanical systems using switching and saturation. In *Proceedings of the block island workshop on control using logic based switching*.

Srinivasan, B., Huguenin, P., & Bonvin, D. (2009). Global stabilization of an inverted pendulum-control strategy and experimental verification. *Automatica*, *45*, 265–269.

Teel, A. (1996). A nonlinear small gain theorem for the analysis of control system with saturation. *IEEE Transactions on Automatic Control*, *41*, 1256–1270.

Xu, J., Guo, Z., & Lee, T. H. (2013). Design and implementation of integral sliding-mode control on an underactuated two-wheeled mobile robot. *ISA Transactions*, *58*, 870–880.

Joonho Lee received the B.S. degree from Dong-a University, Busan, South Korea in 2004, the M.S. degree from Yonsei University, Seoul, South Korea in 2006, and the Ph.D. degree from Michigan State University, East Lansing in 2014, all in mechanical engineering. He was working as Research and Teaching Assistants at Michigan State University, East Lansing, USA.

His research interests are in the areas of nonlinear control, a multi-time-scale approach, underactuated mechanical systems, and extended high-gain observers.

Ranjan Mukherjee received his B.Tech degree from the Indian Institute of Technology, Kharagpur, in 1987; and his M.S. and Ph.D. degrees from the University of California, Santa Barbara, in 1989 and 1991, respectively, all in Mechanical Engineering. Since 1996 he has been with Michigan State University (MSU), where he is currently a Professor in the Department of Mechanical Engineering. Prior to joining MSU, he was an Assistant Professor at the US Naval Postgraduate School in Monterey, California from 1991 to 1996. His research interests lie in the areas of robotics and mechatronics and he has done theoretical and experimental work on nonholonomic systems, mobile and telerobotic systems, under-actuated mechanical systems, walking machines, underwater vehicles, magnetic bearings, flexible structures, and MEMS. Ranjan Mukherjee was an Associate Editor for the ASME Journal of Dynamic Systems, Measurement, and Control from 2001 to 2008 and the ASME Journal of Vibration and Acoustics from 2010 to 2013. He became a Fellow of the ASME in 2008. He is a recipient of the 2008 US Department of State Fulbright Research Scholar Award, the 2011 MSU Withrow Distinguished Senior Scholar Award, and the 2014 ASME Dynamic Systems and Control Division Charles Stark Draper Innovative Practice Award.

Hassan K. Khalil received the B.S. and M.S. degrees in electrical engineering from Cairo University, Egypt, in 1973 and 1975, respectively, and the Ph.D. degree from the University of Illinois, Urbana–Champaign, in 1978, all in electrical engineering.

Since 1978, he has been with Michigan State University (MSU), where he is currently University Distinguished Professor of Electrical and Computer Engineering. He has consulted for General Motors and Delco Products, and published several papers on singular perturbation methods and nonlinear control. He is the author of *Nonlinear Control* (Pearson 2015), *Nonlinear Systems* (Macmillan 1992; Prentice Hall 1996 & 2002) and coauthor of *Singular Perturbation Methods in Control: Analysis and Design* (Academic Press 1986; SIAM 1999).

Dr. Khalil was named IEEE Fellow in 1989 and IFAC Fellow in 2007. He received the 1989 IEEE-CSS George S. Axelby Outstanding Paper Award, the 2000 AACC Ragazzini Education Award, the 2002 IFAC Control Engineering Textbook Prize, the 2004 AACC O. Hugo Schuck Best Paper Award, the 2009 AGEP Faculty Mentor of the Year Award, and the 2015 IEEE-CSS Bode Lecture Prize. At MSU he received the 2003 Teacher Scholar Award, the 1994 Withrow Distinguished Scholar Award, and the 1995 Distinguished Faculty Award. He served as Associate Editor of the IEEE Transactions on Automatic Control, *Automatica*, and *Neural Networks*, and as Editor of *Automatica* for nonlinear systems and control. He was Registration Chair of the 1984 CDC, Finance Chair of the 1987 ACC, Program Chair of the 1988 ACC, and General Chair of the 1994 ACC.